



Article

# Crystal Structure of *Kluyveromyces lactis* Glucokinase (KlGlc1)

Krzysztof M. Zak <sup>1,2</sup>, Magdalena Kalińska <sup>2</sup>, Elżbieta Wątor <sup>2</sup> , Katarzyna Kuśka <sup>2,3</sup>,  
Rościsław Krutyholowa <sup>2,3</sup> , Grzegorz Dubin <sup>2,3</sup>, Grzegorz M. Popowicz <sup>1,4</sup> and  
Przemysław Grudnik <sup>2,\*</sup>

<sup>1</sup> Institute of Structural Biology, Helmholtz Zentrum München, Ingolstädter Landstrasse 1, 85764 Neuherberg, Germany; krzysztof.zak@helmholtz-muenchen.de (K.M.Z.); grzegorz.popowicz@helmholtz-muenchen.de (G.M.P.)

<sup>2</sup> Malopolska Centre of Biotechnology, Jagiellonian University, ul. Gronostajowa 7a, 30-387 Krakow, Poland; guta@friend.pl (M.K.); elkon.wator@gmail.com (E.W.); kуска.kk@gmail.com (K.K.); rostyslav.krutyholova@gmail.com (R.K.); grzegorz.dubin@uj.edu.pl (G.D.)

<sup>3</sup> Faculty of Biochemistry, Biophysics and Biotechnology, Jagiellonian University, ul. Gronostajowa 7, 30-387 Krakow, Poland

<sup>4</sup> Center for Integrated Protein Science Munich at Chair of Biomolecular NMR, Department Chemie, Technische Universität München, Lichtenbergstrasse 4, 85747 Garching, Germany

\* Correspondence: przemyslaw.grudnik@uj.edu.pl

Received: 4 September 2019; Accepted: 25 September 2019; Published: 28 September 2019



**Abstract:** Glucose phosphorylating enzymes are crucial in the regulation of basic cellular processes, including metabolism and gene expression. Glucokinases and hexokinases provide a pool of phosphorylated glucose in an adenosine diphosphate (ADP)- and ATP-dependent manner to shape the cell metabolism. The glucose processing enzymes from *Kluyveromyces lactis* are poorly characterized despite the emerging contribution of this yeast strain to industrial and laboratory scale biotechnology. The first reports on *K. lactis* glucokinase (KlGlc1) positioned the enzyme as an essential component required for glucose signaling. Nevertheless, no biochemical and structural information was available until now. Here, we present the first crystal structure of KlGlc1 together with biochemical characterization, including substrate specificity and enzyme kinetics. Additionally, comparative analysis of the presented structure and the prior structures of *lactis* hexokinase (KlHxk1) demonstrates the potential transitions between open and closed enzyme conformations upon ligand binding.

**Keywords:** *Kluyveromyces lactis*; glucokinase; sugar metabolism

## 1. Introduction

Glucose is one of the main factors in metabolism and key regulators of gene expression in eukaryotic organisms, including yeast, protists, plants, and mammals. Glucose-dependent regulation requires glucose phosphorylation provided by glucose-phosphorylating enzymes, glucokinases, and hexokinases. These enzymes are responsible for intracellular trapping and metabolism initiation of monosaccharides and catalyze ATP-driven phosphorylation, yielding ADP and glucose-6-phosphate. Glucose phosphorylation is also considered as drug target against parasitic protists [1–3]. Additionally, some ADP-dependent sugar kinases were also characterized, but their role remains more elusive [4–6].

In yeast, plant and mammalian cells' sugar kinases were shown to be responsible for glucose sensing and signaling [7–10], positioning those enzymes as providers of a carbon source and regulators of sugar-dependent cellular mechanisms. A number of hexokinases were demonstrated to translocate to the nucleus and intercede in the process of glucose repression of transcription in yeast [11] and plants [12]. In mammals, hexokinases have been shown to play a role in the mechanisms of sugar

homeostasis [13]. Although the hexokinase interacting partners were shown to play a critical role in the activity of those enzymes [11,12,14,15], the limited structural information and lack of in vivo studies hinder the complete understanding of hexokinase role in nutrient signaling [16–18].

*Kluyveromyces lactis* is an emerging tool in biotechnology. Since the early 1990s, it has been employed as a host for recombinant protein expression for industrial use (summarized in [19]). One of the most important examples relates to its use in industrial production of lactase and bovine chymosin, enzymes which are important in food biotechnology [20]. Due to the growing importance of *K. lactis* in biotechnology, research on biology and metabolism of this microorganism gains value for both scientific and industrial reasons.

KlGlk1 was reported for the first time by Kettner and colleagues [21]. The group identified the KLLA0C01155g gene in *K. lactis* genome on the basis of its high similarity to *Saccharomyces cerevisiae* glucokinase (ScGlk1, nucleotide identity 62.4%) and glucokinase-like protein ScEMI2 (nucleotide identity 63.3%) genes. Genomic analysis, followed by isolation and functional analysis of the protein, revealed its enzymatic activity and specificity. The KlGlk1 mutants denoted the role of the enzyme as an accessory glucose phosphorylating protein (to KlHxk1) which might act as a glucose phosphorylation enzyme with currently unknown physiological function.

So far, KlHxk1 hexokinase is the only structurally characterized sugar metabolizing enzyme from *K. lactis* [22–24]. Here, we extend the structural understanding of *K. lactis* glucose phosphorylating enzymes. We have expressed and purified recombinant KlGlk1 and solved its crystal structure at 2.6 Angstrom (Å) resolution. Comparative analysis of the structure of KlGlk1 reported in this study and the prior structure of KlHxk1 demonstrates the transitions between open and closed enzyme conformations.

## 2. Results and Discussion

### 2.1. Biochemical Characterization

We have recombinantly expressed, purified, and crystalized KlGlk1 glucokinase from *K. lactis* and characterized its enzymatic properties. First, we analyzed the protein's thermal stability using both thermal shift assay (TSA) and Tycho analysis (Figure S1). Using these methods, the unfolding temperatures were determined at  $41.9 \pm 0.1$  °C and  $53.6 \pm 0.05$  °C for TSA and Tycho, respectively. Values obtained by TSA and Tycho cannot be directly compared due to different temperature gradients and readout methodology used by both techniques, although both document relatively low thermal stability of the protein.

Next, we assayed the protein activity using constant ATP concentration equal to 0.5 mM and the standard Michaelis–Menten model to quantify the affinity ( $K_m$ ) for glucose (Figure 1A). Tested conditions yielded the apparent kinetic parameters  $k_{cat(app)} = 150 \text{ s}^{-1}$  and  $K_{m(app)} = 0.08 \text{ mM}$ .

In the previous work, Kuettner and colleagues observed that *K. lactis* JA6Δrag5 strain lacking KlHxk1 hexokinase revealed significant growth on glucose, but not on fructose. Thus, we tested KlGlk1's ability to catalyze phosphate transfer from ATP to fructose, and we observed no such activity at tested conditions.

Sugar kinases often exhibit inhibition by ATP. The phenomenon of substrate inhibition has been described for hexokinases which may be inhibited even by physiological concentrations of ATP [25]. Hence, we tested if KlGlk1 is prone to substrate inhibition by ATP at a concentration above 0.25 mM (Figure 1B). We used fixed glucose concentration (0.5 mM) to determine the apparent kinetic parameters ( $k_{cat(app)} = 400 \text{ s}^{-1}$ ,  $K_{m(app)} = 0.15 \text{ mM}$ ) of KlGlk1 for ATP concentrations preceding substrate inhibition range. Comparative fitting of a standard Michaelis–Menten model with and without Hill coefficient (Figure S2A,B) revealed strong positive cooperativity at low ATP concentrations as indicated by the Hill coefficient of 1.97 determined from the  $V = V_{max} \cdot [ATP]^h / (K_m^h + [ATP]^h)$  equation. Sigmoidal shape of the Hill plot (Figure S2C) suggests that KlGlk1 exists in two states with different catalytic activity, with an apparent transition point at 45 μM ATP. At higher ATP concentrations, abnormally

strong substrate inhibition takes place, which in pair with positive cooperativity observed in case of *KlGlk1* could be explained, among others, by protein dimerization. To fit the theoretical model to our data, we combined the classical Yoshino and Murakami substrate inhibition model of a complete type, which was previously validated on *Escherichia coli* phosphofructokinase II, with a kinetic model derived for dimerizing enzymes [26,27]. Interestingly, numerical values of  $k_{cat}$  and  $K_m$  calculated based on this model do not differ significantly from values estimated by classical Michaelis–Menten kinetics for a lower concentration range. The ratio of a substrate inhibition constant to a Michaelis–Menten constant ( $K_{si}/K_m$ ) is close to 1.0, indicating a substrate inhibition of a complete type, which means that at high substrate concentrations, the  $[ES_1S_2]_2$  complex is formed, and it is unable to perform the reaction. As stated previously, strong substrate inhibition of *KlGlk1* may be explained, among others, by protein dimerization. Therefore, we investigated the possible dimerization using size-exclusion chromatography coupled to light scattering (right-angle light scattering/low-angle light scattering (RALS/LALS)). Analysis of RALS/LALS distribution demonstrated that *KlGlk1* elutes as a dimer of apparent molecular weight of 100 kDa (Figure S3). This observation goes in line with size-exclusion chromatography retention time calibrated with molecular weight standards.

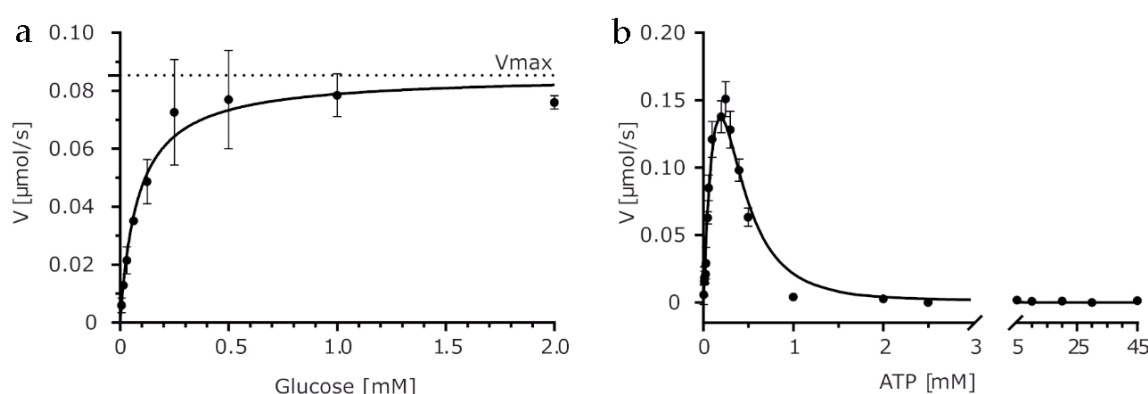


**Figure 1.** Kinetic analysis of *KlGlk1* activity. **(a)** Reaction velocity as a function of glucose concentration measured at 0.5 mM ATP. Solid line represents fit of standard Michaelis–Menten model,  $R^2 = 0.98$ ;  $V_{max}$  ( $0.085 \pm 0.004 \mu\text{M/s}$ ; dotted line),  $k_{cat}$  (app) ( $150 \text{ s}^{-1}$ )  $K_m$  ( $0.082 \pm 0.013 \text{ mM}$ ). Error bars correspond to SD,  $N = 3$ . **(b)** Reaction velocity as a function of ATP concentration measured at 0.5 mM glucose. Substrate inhibition is clearly visible starting from 0.25 mM ATP. Solid line indicates a substrate inhibition model with a correction for dimerization,  $R^2 = 0.97$ . Error bars correspond to SD,  $N = 3$ .

## 2.2. Overall Structure

We crystallized *KlGlk1* in an apo form. The crystal structure of *KlGlk1* was determined by molecular replacement pipeline MoRDa using Protein Data Bank (PDB) entry 3O8M as a search model [28]. The structure was refined to  $R_{work}/R_{free}$  values of 0.205/0.244 at 2.6 Å resolution (Table 1). The asymmetric unit contains three *KlGlk1* molecules and the unit cell belongs to  $C 2 2_1$  space group (Figure 2a).

*KlGlk1* consists of two ribonuclease H-like type domains (Figure 2b, Figures S4 and S5). The N-terminal, smaller domain K represents compact fold with beta strands in the domain's core and short alpha helices located between strands 1–3 and 10–13 as well as at the top of domain K (helices 3 and 4). Larger domain Z consists of central mixed  $\beta$ -sheet (strands 10–13) flanked by alpha helices connected by the extended loops resulting in the elongated shape of the domain. Inspection of the overlap among the molecules contained in the asymmetric unit (ASU) does not indicate any significant structural differences as confirmed by low root mean square deviation (RMSD) values calculated by TM-align (RMSD calculated based on backbone C alpha atoms; RMSD values of backbone atoms of chains A/B, B/C and A/C are 0.53 for 469 residues, 0.62 for 469 residues, 0.54 for 470 residues, respectively) [29]. Two out of three *KlGlk1* monomers (chains B and C) create relatively large contacts

in the crystal, resulting in a total buried area of  $372.6 \text{ \AA}^2$  (interaction surfaces were calculated using the PISA server) [30]. The third molecule (chain A) creates less significant contacts only with monomer B, resulting in a total buried area of  $87.1 \text{ \AA}^2$ . Nonetheless, this analysis of the arrangement of molecules in the crystal does not indicate stable dimerization—the buried surface areas are too small to ensure stable dimerization in solution. This is confirmed by automated analysis criteria implemented in the PISA server, suggesting no formation of stable quaternary structures, thereby indicating protein's monomeric state in the presented crystal structure [30].

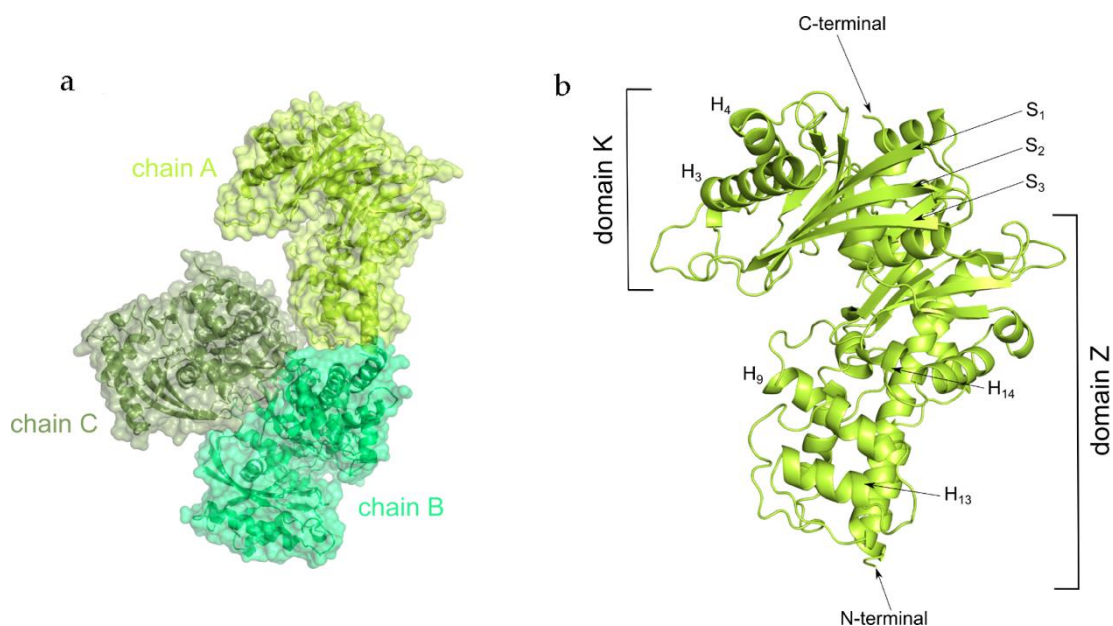


**Figure 2.** Crystal structure of *KIGlk1*. (a) Arrangement of *KIGlk1* molecules in the asymmetric unit. (b) Architecture of *KIGlk1* monomer (chain A). H indicates helices, S indicates strands.

### 2.3. Structural Comparison between *KIGlk1* and *KIHxk1* Glucokinases

*KIHxk1*, the closest homolog of *KIGlk1*, was crystallized in several different crystal forms showing the monomeric and dimeric states of the enzyme [23,24]. The structures of dimeric *KIHxk1* show that protein forms a symmetrical, ring-shaped homodimer with a head-to-tail arrangement of the protein molecules. The structures of apo and substrate (glucose) bound forms provided molecular insight into the mechanism of substrate binding and related conformational changes.

Comparative analysis of the *KIGlk1* structure and available *KIHxk1* Protein Data Bank (PDB) entries presenting the later protein in open state shows significant similarities in the overall structure despite low amino acid sequence identity (Figure S6). Superposition of *KIGlk1* and *KIHxk1* in open state (PDB 3O08) demonstrate almost identical fold and position of both domains. Only small differences are noticeable in the loop regions between residues 135–145, 330–347, and 412–422, most probably due to the flexible nature of these parts characterized by high B factors (Figure S7). More pronounced differences are visible in the 246–266 region, where *KIHxk1* folds into a helix flanked by unstructured regions compared to the long, unstructured loop in the *KIHxk1*, as well as between 450–462 residues of *KIGlk1* where the loop region with an inserted short helix is significantly shorter in *KIGlk1* than in *KIHxk1* (*KIGlk1* residues 450–462 corresponds to residues 437–453 of *KIHxk1*).

The crystal structures of *KIHxk1* reported previously indicate that hexokinase undergoes profound conformational changes upon substrate binding [23]. Superposition of the structure of *KIGlk1* reported in this study and the structure of *KIHxk1* in a closed, substrate bound conformation (PDB 3O8M; Figure 3) suggests that *KIGlk1* structure has been determined in its open state (accordingly, no substrate is present at the active site). Superposition and detailed comparison shows that the relative arrangement of small and large domains in *KIGlk1* and substrate bound *KIHxk1* is different. In *KIHxk1*, the substrate



binding promotes the closed conformation of protein, whereas apo *KlGlc1* remains in open state. This phenomenon is typical for sugar phosphorylating proteins and has been described before [5,31]. The difference in protein conformation and domain location supports our suggestion concerning *KlGlc1* open state. Moreover, the protein part undergoing conformational change encompasses the region of 115–195 residues that folds into helices H<sub>3</sub> and H<sub>4</sub> and stands S<sub>4</sub>–S<sub>7</sub> with a 165–174 loop that might be responsible for stabilizing the substrate at the active site of the enzyme.

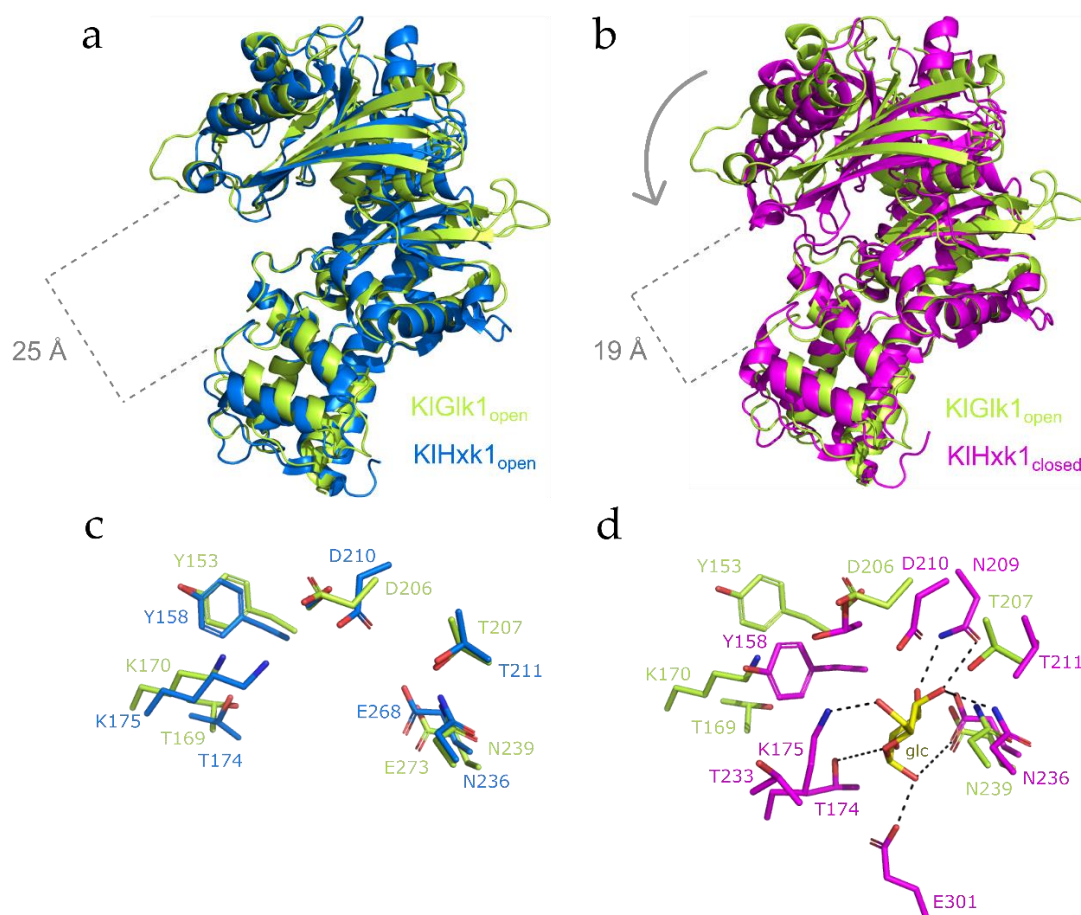


**Figure 3.** Comparison of crystal structures of *KlGlc1* and *KlHxk1* kinases. (a) Superposition of *KlGlc1* and *KlHxk1* (PDB:3o08) in open states. (b) Superposition of *KlGlc1* in the open state and *KlHxk1* in the closed state (PDB:3o8m). (c) Superposition of active site residues of *KlGlc1* and *KlHxk1* in open state (PDB:3o08). (d) Superposition of active site residues of *KlGlc1* and *KlHxk1* in closed state (PDB:3o8m). Superpositions were made over large domains of *KlGlc1* and *KlHxk1* (TM-align module in PyMol software, residues 2–60 and 220–481 for *KlGlc1*, residues 15–60 and 220–484 for *KlHxk1*).

We report here a *KlGlc1* crystal structure in an open conformation. The kinetic assays performed on recombinant protein confirmed protein activity towards glucose and no activity towards fructose. We also observed a relatively strong substrate inhibition by ATP in the concentration range exceeding 0.25 mM. This indicates a tight regulation of *KlGlc1* by ATP. The protein remains inactive when the ATP level in the cell is high, which suggests that *KlGlc1* serves as a safety mechanism preventing too fast energy production. Both kinetic analysis and light scattering studies show that *KlGlc1* forms a dimer in solution, which is likely related to activity regulation by ATP.

### 3. Materials and Methods

#### 3.1. Cloning, Expression and Purification

The *Kluyveromyces lactis* KLLA0C01155g gene was codon optimized for improved expression in *Escherichia coli*. The gene was synthesized (GenScript, Leiden, Netherlands) and subcloned to a pET24d expression vector. N-terminal His-tagged KIGlk1 was expressed in *E. coli* BL21 (DE3) using terrific broth medium supplemented with kanamycin. Briefly, cells were cultivated until OD<sub>600</sub> value of 1 at 37 °C, the expression was induced with 0.5 mM isopropyl-β-D-thiogalactoside (IPTG), and cultures were incubated for 16 h at 16 °C. After expression, cells were collected and resuspended in lysis buffer containing 150 mM NaCl, 20 mM imidazole, 20 mM (4-(2-hydroxyethyl)-1-piperazineethanesulfonic acid) (HEPES) pH 8.0 and lysed by sonication. Soluble fraction was loaded onto Ni-Sepharose (GE Healthcare, Uppsala, Sweden) column equilibrated with lysis buffer. Protein was eluted with lysis buffer containing 500 mM imidazole and mixed with Tobacco etch virus (TEV) protease. After incubation, solution was loaded onto Ni-Sepharose resin to remove His-tag and TEV protease. Finally, KIGlk1 was concentrated and purified to homogeneity by gel filtration using Superdex 75 (GE Healthcare, Uppsala, Sweden) in 150 mM NaCl, 20 mM HEPES, pH 8.0 (Figure S8). Fractions containing protein of interest were pooled and concentrated to 10 mg/mL.

#### 3.2. Crystallization and Structure Determination

Crystallization screening was carried out using commercially available buffer sets (Molecular Dimensions) in a sitting-drop vapor diffusion setup by mixing 1 µL of protein solution and 1 µL of buffer solution at room temperature. Diffraction quality crystals were obtained from condition containing 0.15 M potassium bromide and 30% (*w/v*) poly(ethylene glycol) (PEG) monomethyl ether (MME) 2000. Crystals were cryoprotected with 30% ethylene glycol in mother liquor and flash frozen in liquid nitrogen.

Diffraction data were collected at 14.1 beamline at BESSY II, Berlin, Germany [32] using Pilatus 6M detector to 2.6 Å resolution (Table 1). The data were indexed and integrated using XDS [33] then scaled and merged using Scala [34]. Structure was solved using MoRDa server [28] and Phaser [35] using PDB 3O8M as a search model. As the search model shared only 38% of its amino acid sequence identity with KIGlk1, several parts of the model were manually rebuilt using Coot [36]. Restrained refinement was performed using Phenix [37]. Five percent of the reflections were used for cross-validation analysis, and the behavior of the R<sub>free</sub> was employed to monitor the refinement strategy. Water molecules were added using Coot and subsequently manually inspected. The loop containing residues 43–48 (chain A; 43–49 for chain B) was not fully resolved in the electron density map and therefore was not modeled. The final model comprises residues 2–481 from each monomer and 196 water molecules.

**Table 1.** Data collection and refinement statistics.

KIGlk1 (PDB 6R2N)	
Data Collection	
Space group	C 2 2 2 <sub>1</sub>
Total reflections/Unique reflections	139134 (13371)
Cell dimensions	102.0 Å, 122.7 Å, 360.3 Å 90°, 90°, 90°
Wavelength (Å)	0.9184
Resolution (Å)	49.08–2.596 (2.689–2.596)
Mean I/sigma (I)	13.6 (1.7)
Completeness (%)	99.58 (97.10)
Multiplicity	2.0 (2.0)
CC <sub>1/2</sub>	98.6 (52.8)

Table 1. Cont.

KlGlk1 (PDB 6R2N)	
<b>Refinement</b>	
Reflections used in refinement	69952 (6762)
Reflections used for R-free	1099 (107)
R-work	0.2045 (0.3300)
R-free	0.2396 (0.3345)
<b>Number of Atoms/Molecules</b>	
non-hydrogen atoms	11273
macromolecules	11032
ligands♦	45
solvent	196
<b>B-factors</b>	
average B-factor (Å)	76.69
macromolecules (Å)	77.06
ligands (Å)	86.48
solvent (Å)	53.66
wilson B-factor (Å)	53.71
<b>Ramachandran plot</b>	
Ramachandran favored (%)	96.88
Ramachandran allowed (%)	3.05
Ramachandran outliers (%)	0.07
<b>R. m. s. deviations</b>	
Bonds (Å)	0.004
Angles (°)	0.96
Rotamer outliers (%)	0.92
Clashscore	3.08

Values in parentheses are for high resolution shell. ♦ Ligands in the presented structure include chemicals from crystallization condition and cryoprotectant solution and are not biologically relevant in the presented context.

### 3.3. Activity Assay

KlGlk1 activity was assessed by monitoring the level of one of the reaction products (glucose-6-phosphate) in a coupled glucose-6-phosphate dehydrogenase (G6PD) reaction essentially as described previously [5,6]. Unless stated otherwise, the assays were performed at 37 °C in reaction buffer (20 mM Tris-HCl pH 7.4, 250 mM sucrose, 50 mM KCl, 5 mM MgCl<sub>2</sub>) supplemented with glucose-6-phosphate dehydrogenase (1 unit) and nicotinamide adenine dinucleotide phosphate (NADP) (0.5 mM). The KlGlk1 protein concentration was adjusted to 0.16 mg/mL (3 µM).

### 3.4. RALS/LALS Analysis

The oligomeric state of KlGlk1 was investigated by size-exclusion chromatography (Superdex 200 Increase 10/300 GL column) coupled to right-angle light scattering (RALS) followed by measurement of refractive index (RI) using OMNISEC REVEAL. Measurements were performed in 50 mM Tris pH 7.8, 200 mM NaCl, 5 mM β-ME buffer, and results were analyzed using OMNISEC software.

### 3.5. Protein Stability Analysis

Melting points (T<sub>m</sub>-values) of KlGlk1 glucokinase were obtained using thermal shift assay (TSA) and real time monitoring of changes in the intrinsic protein fluorescence by Tycho NT.6 [38]. For TSA analysis, KlGlk1 (1 mg/mL) was incubated with Sypro Orange dye in 150 mM NaCl, 20 mM HEPES, pH 8.0. Fluorescence signal of Sypro Orange was determined as a function of temperature between 5 and 95 °C in increments of 1.2 °C/min. The melting temperature was calculated as the inflexion point of the fluorescence vs. temperature function. Each experiment was carried out in triplicate. For Tycho NT.6 analysis, capillary was loaded with 10 µL of KlGlk1 (1 mg/mL) in 150 mM NaCl, 20 mM HEPES,

pH 8.0 and heated from 35 to 95 °C in 3 min overall time. The melting temperature was calculated as the inflexion point of the 350 nm/330 nm intrinsic fluorescence vs. temperature function.

### 3.6. Protein Data Bank Accession Code

Coordinates and structure factors for the KIGlk1 have been deposited in Protein Data Bank (PDB) with code 6R2N.

## 4. Conclusions

Our study expands the understanding of glucose metabolizing enzymes in *K. lactis* by presenting the first crystal structure of its unique glucokinase. The KIGlk1 structure along with the biochemical data help to understand the mechanisms responsible for glucose sensing and signaling, therefore allowing for more intensive use of *K. lactis* for both scientific and industrial applications.

**Supplementary Materials:** Supplementary materials can be found at <http://www.mdpi.com/1422-0067/20/19/4821/s1>.

**Author Contributions:** P.G. designed and initiated the research; M.K. expressed and purified the protein; K.M.Z., E.W., and P.G. collected X-ray diffraction data and solved and refined the structure; K.K. performed activity assays; R.K. analyzed enzyme kinetics data; G.D. and G.M.P. provided key reagents; K.M.Z., E.W., and P.G. wrote the manuscript. All authors commented on the final draft.

**Funding:** The research has been supported by National Science Centre research grant no. UMO-2015/19/D/NZ1/02009 to P.G. and no. UMO-2012/07/E/NZ1/01907 to G.D., EU HORIZON 2020 ITN AEGIS to GP and GD. We acknowledge the MCB Structural Biology Core Facility (supported by the TEAM TECH CORE FACILITY/2017-4/6 grant from the Foundation for Polish Science) for valuable support.

**Acknowledgments:** The X-ray data were collected at the BESSY II 14.1 beamline at Helmholtz-Zentrum Berlin für Materialien und Energie (HZB). We would like to thank Dr. Piotr Wilk for the invaluable help with structure refinement and Dr. Artur Biela for help with light scattering measurements.

**Conflicts of Interest:** Authors declare no conflict of interest.

## Abbreviations

ATP	Adenosine triphosphate
ADP	Adenosine diphosphate
Å	Angstrom
TSA	Thermal Shift Assay
RMSD	Root Mean Square Deviation
IPTG	Isopropyl-β-D-thiogalactoside
HEPES	(4-(2-hydroxyethyl)-1-piperazineethanesulfonic acid)
PEG	Poly(ethylene glycol)
RALS/LALS	Right-angle light scattering/low-angle light scattering
TRIS	Trisaminomethane
NADP	Nicotinamide adenine dinucleotide phosphate

## References

1. Merritt, C.; Silva, L.E.; Tanner, A.L.; Stuart, K.; Pollastri, M.P. Kinases as druggable targets in trypanosomatid protozoan parasites. *Chem. Rev.* **2014**, *114*, 11280–11304. [\[CrossRef\]](#) [\[PubMed\]](#)
2. Flaherty, D.P.; Harris, M.T.; Schroeder, C.E.; Khan, H.; Kahney, E.W.; Hackler, A.L.; Patrick, S.L.; Weiner, W.S.; Aube, J.; Sharlow, E.R.; et al. Optimization and Evaluation of Antiparasitic Benzamidobenzoic Acids as Inhibitors of Kinetoplastid Hexokinase 1. *ChemMedChem* **2017**, *12*, 1994–2005. [\[CrossRef\]](#) [\[PubMed\]](#)
3. Kalel, V.C.; Mäser, P.; Sattler, M.; Erdmann, R.; Popowicz, G.M. Come, sweet death: Targeting glycosomal protein import for antitrypanosomal drug development. *Curr. Opin. Microbiol.* **2018**, *46*, 116–122. [\[CrossRef\]](#) [\[PubMed\]](#)
4. Ito, S.; Fushinobu, S.; Jeong, J.J.; Yoshioka, I.; Koga, S.; Shoun, H.; Wakagi, T. Crystal structure of an ADP-dependent glucokinase from *Pyrococcus furiosus*: implications for a sugar-induced conformational change in ADP-dependent kinase. *J. Mol. Biol.* **2003**, *331*, 871–883. [\[CrossRef\]](#)



5. Grudnik, P.; Kaminski, M.M.; Rembacz, K.P.; Kuska, K.; Madej, M.; Potempa, J.; Dawidowski, M.; Dubin, G. Structural basis for ADP-dependent glucokinase inhibition by 8-bromo-substituted adenosine nucleotide. *J. Biol. Chem.* **2018**, *293*, 11088–11099. [[CrossRef](#)] [[PubMed](#)]
6. Tokarz, P.; Wisniewska, M.; Kaminski, M.M.; Dubin, G.; Grudnik, P. Crystal structure of ADP-dependent glucokinase from *Methanocaldococcus jannaschii* in complex with 5-iodotubercidin reveals phosphoryl transfer mechanism. *Protein Sci.* **2018**, *27*, 790–797. [[CrossRef](#)] [[PubMed](#)]
7. Entian, K.D. Genetic and biochemical evidence for hexokinase PII as a key enzyme involved in catabolite repression in yeast. *Mol. Gen. Genet.* **1980**, *178*, 633–637. [[CrossRef](#)]
8. Rolland, F.; Winderickx, J.; Thevelein, J.M. Glucose-sensing mechanisms in eukaryotic cells. *Trends Biochem. Sci.* **2001**, *26*, 310–317. [[CrossRef](#)]
9. Rolland, F.; Baena-Gonzalez, E.; Sheen, J. Sugar sensing and signaling in plants: conserved and novel mechanisms. *Annu. Rev. Plant. Biol.* **2006**, *57*, 675–709. [[CrossRef](#)]
10. Wilson, J.E. Isozymes of mammalian hexokinase: structure, subcellular localization and metabolic function. *J. Exp. Biol.* **2003**, *206*, 2049–2057. [[CrossRef](#)]
11. Moreno, F.; Ahuatzi, D.; Riera, A.; Palomino, C.A.; Herrero, P. Glucose sensing through the Hxk2-dependent signalling pathway. *Biochem. Soc. Trans.* **2005**, *33*, 265–268. [[CrossRef](#)] [[PubMed](#)]
12. Cho, Y.H.; Yoo, S.D.; Sheen, J. Regulatory functions of nuclear hexokinase 1 complex in glucose signaling. *Cell* **2006**, *127*, 579–589. [[CrossRef](#)] [[PubMed](#)]
13. Postic, C.; Shiota, M.; Magnuson, M.A. Cell-specific roles of glucokinase in glucose homeostasis. *Recent Prog. Horm. Res.* **2006**, *56*, 195–217. [[CrossRef](#)]
14. van Schaftingen, E.; Veiga-da-Cunha, M.; Niculescu, L. The regulatory protein of glucokinase. *Biochem. Soc. Trans.* **1997**, *25*, 136–140. [[CrossRef](#)] [[PubMed](#)]
15. de la Cera, T.; Herrero, P.; Moreno-Herrero, F.; Chaves, R.S.; Moreno, F. Mediator factor Med8p interacts with the hexokinase 2: implication in the glucose signalling pathway of *Saccharomyces cerevisiae*. *J. Mol. Biol.* **2002**, *319*, 703–714. [[CrossRef](#)]
16. Anderson, C.M.; McDonald, R.C.; Steitz, T.A. Sequencing a protein by x-ray crystallography. I. Interpretation of yeast hexokinase B at 2.5 Å resolution by model building. *J. Mol. Biol.* **1978**, *123*, 1–13. [[CrossRef](#)]
17. Bennett, W.S., Jr.; Steitz, T.A. Structure of a complex between yeast hexokinase A and glucose. II. Detailed comparisons of conformation and active site configuration with the native hexokinase B monomer and dimer. *J. Mol. Biol.* **1980**, *140*, 211–230. [[CrossRef](#)]
18. Kuser, P.R.; Krauchenco, S.; Antunes, O.; Polikarpov, I. The high resolution crystal structure of yeast hexokinase PII with the correct primary sequence provides new insights into its mechanism of action. *J. Biol. Chem.* **2000**, *275*, 20814–20821. [[CrossRef](#)] [[PubMed](#)]
19. Spohner, S.C.; Schaum, V.; Quitmann, H.; Czermak, P. *Kluyveromyces lactis*: An emerging tool in biotechnology. *J. Biotechnol.* **2016**, *222*, 104–116. [[CrossRef](#)]
20. van Ooyen, A.J.; Dekker, P.; Huang, M.; Olsthoorn, M.M.; Jacobs, D.I.; Colussi, P.A.; Taron, C.H. Heterologous protein production in the yeast *Kluyveromyces lactis*. *FEMS Yeast Res.* **2006**, *6*, 381–392. [[CrossRef](#)]
21. Kettner, K.; Müller, E.C.; Otto, A.; Rödel, G.; Breunig, K.D.; Kriegl, T.M. Identification and characterization of a novel glucose-phosphorylating enzyme in *Kluyveromyces lactis*. *FEMS Yeast Res.* **2007**, *7*, 683–692. [[CrossRef](#)] [[PubMed](#)]
22. Kuettner, E.B.; Kriegl, T.M.; Keim, A.; Naumann, M.; Sträter, N. Crystallization and preliminary X-ray diffraction studies of hexokinase KIHxk1 from *Kluyveromyces lactis*. *Acta Crystallogr. Sect. F Struct. Biol. Cryst. Commun.* **2007**, *63*, 430–433. [[CrossRef](#)] [[PubMed](#)]
23. Kuettner, E.B.; Kettner, K.; Keim, A.; Svergun, D.I.; Volke, D.; Singer, D.; Hoffmann, R.; Müller, E.C.; Otto, A.; Kriegl, T.M.; et al. Crystal structure of hexokinase KIHxk1 of *Kluyveromyces lactis*: a molecular basis for understanding the control of yeast hexokinase functions via covalent modification and oligomerization. *J. Biol. Chem.* **2010**, *285*, 41019–41033. [[CrossRef](#)] [[PubMed](#)]
24. Kettner, K.; Kuettner, E.B.; Otto, A.; Lilie, H.; Golbik, R.P.; Sträter, N.; Kriegl, T.M. In vivo phosphorylation and in vitro autophosphorylation-inactivation of *Kluyveromyces lactis* hexokinase KIHxk1. *Biochem. Biophys. Res. Commun.* **2013**, *435*, 313–318. [[CrossRef](#)] [[PubMed](#)]
25. Kopetzki, E.; Entian, K.D. Glucose repression and hexokinase isoenzymes in yeast. Isolation and characterization of a modified hexokinase PII isoenzyme. *Eur. J. Biochem.* **1985**, *146*, 657–662. [[CrossRef](#)] [[PubMed](#)]

26. Yoshino, M.; Murakami, K. Analysis of the substrate inhibition of complete and partial types. *Springerplus* **2015**, *4*, 292. [[CrossRef](#)] [[PubMed](#)]
27. Ishikawa, H.; Ogino, H.; Oshida, H. Rates of reactions catalysed by a dimeric enzyme. Effects of the reaction scheme and the kinetic parameters on co-operativity. *Biochem. J.* **1991**, *280*, 131–137. [[CrossRef](#)] [[PubMed](#)]
28. Vagin, A.; Lebedev, A. MoRDa, an automatic molecular replacement pipeline. *Acta Cryst. A* **2015**, *71*, 19. [[CrossRef](#)]
29. Zhang, Y.; Skolnick, J. TM-align: A protein structure alignment algorithm based on TM-score. *Nucl. Acids Res.* **2005**, *33*, 2302–2309. [[CrossRef](#)]
30. Krissinel, E.; Henrick, K. Inference of macromolecular assemblies from crystalline state. *J. Mol. Biol.* **2007**, *372*, 774–797. [[CrossRef](#)]
31. Rivas-Pardo, J.A.; Herrera-Morande, A.; Castro-Fernandez, V.; Fernandez, F.J.; Vega, M.C.; Guixé, V. Crystal Structure, SAXS and Kinetic Mechanism of Hyperthermophilic ADP-Dependent Glucokinase from *Thermococcus litoralis* reveal a Conserved Mechanism for Catalysis. *PLoS ONE* **2013**, *8*, e66687. [[CrossRef](#)] [[PubMed](#)]
32. Mueller, U.; Förster, R.; Hellmig, M.; Huschmann, F.U.; Kastner, A.; Malecki, P.; Pühringer, S.; Röwer, M.; Sparta, K.; Steffien, M.; et al. The macromolecular crystallography beamlines at BESSY II of the Helmholtz-Zentrum Berlin: Current status and perspectives. *Eur. Phys. J. Plus* **2015**, *130*, 141–150. [[CrossRef](#)]
33. Kabsch, W. XDS. *Acta Crystallogr. D Biol. Crystallogr.* **2010**, *66*, 125–132. [[CrossRef](#)] [[PubMed](#)]
34. Evans, P.R. Scaling and assessment of data quality. *Acta Crystallogr. D Biol. Crystallogr.* **2006**, *62*, 72–82. [[CrossRef](#)] [[PubMed](#)]
35. McCoy, A.J.; Grosse-Kunstleve, R.W.; Adams, P.D.; Winn, M.D.; Storoni, L.C.; Read, R.J. Phaser crystallographic software. *J. Appl. Crystallogr.* **2007**, *40*, 658–674. [[CrossRef](#)]
36. Emsley, P.; Lohkamp, B.; Scott, W.G.; Cowtan, K. Features and development of Coot. *Acta Crystallogr. D Biol. Crystallogr.* **2010**, *66*, 486–501. [[CrossRef](#)]
37. Adams, P.D.; Afonine, P.V.; Bunkóczi, G.; Chen, V.B.; Davis, I.W.; Echols, N.; Headd, J.J.; Hung, L.W.; Kapral, G.J.; Grosse-Kunstleve, R.W.; et al. PHENIX: a comprehensive Python-based system for macromolecular structure solution. *Acta Crystallogr. D Biol. Crystallogr.* **2010**, *66*, 213–221. [[CrossRef](#)]
38. Reinhard, L.; Mayerhofer, H.; Geerlof, A.; Mueller-Dieckmann, J.; Weiss, M.S. Optimization of protein buffer cocktails using Thermofluor. *Acta Crystallogr. Sect. F Struct. Biol. Cryst. Commun.* **2013**, *69*, 209–214. [[CrossRef](#)]



© 2019 by the authors. Licensee MDPI, Basel, Switzerland. This article is an open access article distributed under the terms and conditions of the Creative Commons Attribution (CC BY) license (<http://creativecommons.org/licenses/by/4.0/>).